JOURNAL OF NEUROPHYSIOLOGY
Vol. 65, No. 3, March 1991. *Printed in U.S.A.*

Spatiotemporal Mechanisms in Receptive Fields of Visual Cortical Simple Cells: A Model

FLORENTIN WÖRGÖTTER AND GARY HOLT
California Institute of Technology, Computation and Neural Systems Program, Pasadena, California 91125

SUMMARY AND CONCLUSIONS

1. Simple cells in the visual cortex have been subdivided into nondirection-selective (NDS), direction asymmetric (DA), and direction-selective (DS) cells. DA cells reverse their preferred direction with reversal of the stimulus contrast; DS_2 cells respond with the same preferred direction for light and dark stimuli, whereas DS_1 cells respond only to one (light *or* dark) contrast. Also, four velocity response groups have been distinguished: velocity broadband, low-pass, high-pass, and -tuned cells. This study describes an analytic model of feed-forward spatiotemporal interactions within a receptive field that reproduces these basic features of cortical simple cell behavior in the cat.

2. The spatial structure of the receptive fields is simulated with Gabor functions. Two neurobiologically plausible mechanisms, *temporal low-pass filtering* and *intracortical spatial distribution of activity*, are modeled. The central feature of the study is the implementation of both mechanisms in a spatially continuous way. The model is analytic, but an equivalent neural network diagram was drawn and is used to explain the features of the model.

3. First-order temporal low-pass filtering is performed both after convolving the stimulus light-intensity function with the Gabor type receptive field and also at the final output step of the model. In the circuit diagram this would correspond to low-pass filtering in lateral geniculate nucleus (LGN) and cortical cells. Filtering was adjusted to have a −3-dB drop-off frequency of 2–3 Hz, corresponding to the drop-off frequencies observed in response to temporal modulation of sine-wave gratings.

4. The mechanism that we call *intracortical distribution of activity* is implemented along the axis of stimulus motion. A response elicited from the part of the receptive field that is stimulated at a given time will spread out in the receptive field, influencing regions that have not been stimulated. It is equivalent to spreading of activity on the cortical surface. This mechanism extends the existing ideas of discrete interactions between subfields to a continuous scheme throughout the whole receptive field. It is based on findings that intracortical interactions exist even within single subfields. The impact of distributing the activity is assumed to decrease exponentially with the Euclidian distance between the stimulated region and the region under consideration.

5. Thresholds are implemented only at the level of the cortex. Both the activity distributing mechanism and the output of the cell being studied are thresholded.

6. For odd Gabor functions, mere low-pass filtering without activity distribution and thresholding results in DA cells with velocity low-pass or velocity broadband behavior. Widening the receptive field makes the cells more sensitive to higher velocities.

7. Velocity-tuned DS (DS_1) cells can be modeled by including the activity distribution mechanism. These cells require phase-shifted odd symmetrical receptive fields, which are common among cortical cells.

8. In real cells the response to a moving dot is, in most cases, stronger if the dot moves along the receptive field's long axis than if it moves across. This result is directly reflected in the model with or without activity distribution. The preferred axis of motion for a dot is 90° apart from those for a bar. Reports of shifts in the preferred axis of motion <90° are explained in the model by assuming that the center of rotation of the stimulus was not exactly centered on the excitatory zone of the receptive field.

9. The model predicts that the optimal velocity for a moving dot should always be higher than those for a bar. Also the sharpness of the tuning for a moving dot should increase with increasing velocity, whereas the sharpness of tuning for a bar should decrease.

10. In the present study simple cells are described in an analytic form. The model reproduces the basic spatiotemporal behavior of real cells and makes two predictions that can easily be tested experimentally. In a possible extension of this approach, the computationally simple model cells could be treated as direction- and velocity-selective modules in an artificial neural network architecture.

INTRODUCTION

The *receptive field* of a nerve cell originally was defined as the spatial field that must be stimulated to drive a neuron that receives input from the associated receptors (Hartline 1938). However, the response of a neuron also strongly depends on the temporal pattern of stimulus presentation, so a more complete definition of the receptive field also includes the temporal domain. Following the first descriptions of cell responses in the visual cortex (Hubel and Wiesel 1962), receptive fields have been described in the spatial domain (Daugman 1980, 1984; Field and Tolhurst, 1986; Jones and Palmer 1987a,b; Kulikowski et al. 1982; Marčelja 1980) and also with respect to spatiotemporal interactions (Baker 1988; Baker and Cynader 1986; Bishop et al. 1971; Duysens et al. 1985a,b; Ganz and Felder 1984; Gray et al. 1989; Jones 1970; Mikami et al. 1986; Orban et al. 1981a,b; Pettigrew et al. 1968).

The strongest responses from cortical simple cells in cat are obtained with stimuli consisting of elongated contrast steps (e.g., light bars, edges, or gratings). This behavior gave rise to two different types of models, regarding the cells as either feature detectors (Marr 1982; Marr and Hildreth 1980) or spatial frequency filters (DeValois et al. 1979; Maffei and Fiorentini 1973).

Fine-structure analysis has shown that the spatial domain of simple-cell receptive fields usually includes several elongated ON- and OFF-zones with smooth transients between them and constant distance between their centers (i.e., well-defined spatial frequency) (Jones and Palmer 1987a). In addition, simple cells behave to a large extent linearly (Kulikowski and Bishop 1981). These features have been combined in approaches describing the receptive field with linear spatial filter functions. Gabor functions (Gabor 1946)

have been frequently used because they optimally resolve the trade-off between spatial frequency and orientation resolution (Daugman 1980; Marčelja 1980). In addition, they give a good approximation to the actual shape of simple-cell receptive fields (Field and Tolhurst 1986; Jones and Palmer 1987b). Because nerve cells basically act as half-wave rectifers (they cannot have a negative firing frequency), the filter function approach makes the hidden assumption that at least two half-wave rectifiers with different sign act together to generate the shape of the receptive-field filter function. The cell response (which is the convolution of a *linear* filter with the stimulus) disregards negative values and therefore includes a *nonlinearity*. Such linear-nonlinear (LN) models are widely used (see Pollen and Ronner 1983) and are incorporated into this study.

Models based on Gabor functions focus entirely on the spatial domain. Cortical cells, however, also show temporal properties, the most prominent of which are direction selectivity (Hubel and Wiesel 1962) and velocity tuning (Movshon 1975; Pettigrew et al. 1968). Four subgroups of simple cells have been described on the basis of their responses to various stimulus velocities. Velocity broadband cells respond with constant strength for all but extremely slow or fast velocities. Velocity low-pass cells show a smaller response to larger velocities, whereas the reverse is true for velocity high-pass cells. Velocity-tuned cells show a large response to a particular velocity and a smaller response to velocities on either side (Orban et al. 1981a). Velocity broadband, low-pass, and high-pass cells usually exhibit weak direction tuning, whereas velocity-tuned cells are usually strongly direction selective (Orban et al. 1981a,b; Orban 1984) (see also Table 1). Interactions between subfields can partly account for these response types. For example, several studies showed that feed forward of intracortical inhibition reduces the response in the non-preferred direction (Bishop et al. 1971; Eysel et al. 1987, 1988; Goodwin and Henry 1975; Goodwin et al. 1975; Sillito 1975, 1977); there are, however, also indications that facilitation arises in the preferred direction (Emerson and Gerstein 1977b; Movshon et al. 1978b). Such mechanisms indicate that activity arising from stimulation of a certain region in the visual field does not remain entirely in the retinotopical projection area but is spatially distributed over larger parts of the cortical surface.

Any distribution of activity cannot be purely spatial because of the signal transmission delays between spatially separated interacting cells and their intrinsic low-pass behavior. The low-pass time constants can be determined from the responses to gratings moving at different temporal frequencies (Ikeda and Wright 1975a; Movshon et al. 1978c). Time constants measured in this way are >50 ms, indicating that low-pass filtering in cortical cells is caused by network interactions rather than by temporal integration at the membrane alone, which would result in time constants of ~20 ms.

In a recent study Wörgötter and Eysel (1989) showed that the response of many cat cortical cells to a moving dot is strongest if the dot moves *along the long axis* of the excitatory zone of the receptive field. This axis is approximately orthogonal to the preferred direction of a long bar and has been referred to as the *axial response*.[1] From these results it has been concluded that temporal facilitation occurs along the receptive-field long axis. One possible explanation is that spatiotemporal mechanisms are not limited to interactions between subfields but can also occur within one subfield itself. Thus the response would be facilitated as long as the stimulus travels within an excitatory zone. This idea is supported by the high convergence onto cortical cells, which results in substructure even within individual subfields (Martin 1988).

Many models have been proposed that generate motion-dependent responses. They can be subdivided into models in which the implemented mechanisms are either separable or nonseparable in space and time. Separability means that the impulse response $H_{st}(x, t)$ can be decomposed into $H_{st}(x, t) = H_s(x) \times H_t(t)$, its spatial and temporal components (see Adelson and Bergen 1985). Experimental evidence suggests that separable mechanisms can only account for a weak directional tuning (McLean and Palmer 1989; see, however, Baker and Cynader 1988).

This study combines the spatial structure of the receptive fields (Gabor functions), low-pass behavior, and a mechanism of distributing activity within the receptive field (i.e., distributing activity on the cortical surface) into an analytic model of cortical simple cells. Interactive mechanisms have been discussed for a long time as existing *between* subfields. However, we require that all spatiotemporal interactions occur *continuously* throughout the whole receptive field. This idea is consistent with the high intracortical convergence onto each cell, which accounts for substructure even within subfields. The model consists of two stages, and we show that most aspects of direction, orientation, and velocity tuning as well as axial responses of cortical cells can be reproduced. Experimentally testable predictions are made about the velocity tuning of cells to dot stimulation and about the tuning of cortical cells to nonoptimal bar stimuli. We will discuss the effects of nonseparability on the actual response characteristic of our model and show that weakly directionally tuned cells remain separable, whereas direction selectivity requires a nonseparable mechanism.

TABLE 1. *Various types of velocity response curves and their frequency in cortical cells**

	NDS + DA, %	DS, %	Total, %
Broadband	76	24	21
Low pass	77	23	64
High pass	78	22	4
Tuned	39	61	10

NDS, nondirection selective; DA, directional asymmetrical; DS, directional selective. * Recompiled from Orban (1984).

[1] The term "axial response" in this study is used in a completely different way from the definition of "axial response" given by Henry et al. (1974a). These investigators claimed that the axial response is *parallel* and not orthogonal to the orientational response and that no change in the preferred axis of motion occurs between long and short stimuli. Results from Wörgötter and Eysel (1989) disagree with this finding. An extensive discussion of possible reasons for this discrepancy is given in that paper; we believe that a redefinition of the term axial response is necessary.

Structure of the model

GENERAL OUTLINE. We simulated measurement of orientation and direction tuning of a cell to narrow moving bars. The bar length varied between 0.1 (for a dot) and 10° (for a long bar). Velocity tuning curves were computed with the bar moving along the axis of maximum response.

The schematic diagram in Fig. 1 shows the components of the model. The spatial shape of the receptive field is given by the following odd and even Gabor functions

$$g(x, y) = \exp\left(-\frac{x^2}{2\sigma_x^2} - \frac{y^2}{2\sigma_y^2}\right) \sin(2\pi f_0 x + \phi) \quad (1)$$

or

$$g(x, y) = \exp\left(-\frac{x^2}{2\sigma_x^2} - \frac{y^2}{2\sigma_y^2}\right) \cos(2\pi f_0 x + \phi)$$

In this model the connection pattern that gives rise to the Gabor-like spatial structure of the cortical receptive fields is assumed to be generated at least in part by the convergence of lateral geniculate nucleus (LGN) cell inputs. LGN cells, however, are not explicitly modeled, and they appear in the figure only for display reasons.

We assume that as the signal is passed through LGN it is smoothed by a first-order temporal low-pass filter, becoming

$$C(x, y, t) = \int_0^t I(x, y, t - t')L_L(t')dt' \quad (2)$$

where $L_L(t') = e^{-t'/\tau_L}/\tau_L$, and $I(x, y, t)$ is the stimulus light intensity function (the input to the retina at a point at a particular time).

In our model cortical processing occurs in two layers of units (the top 2 layers of circles in Fig. 1). The hypothesized *activity distribution* arises from the connection pattern between the LGN and the first layer. Activity distribution is a mechanism by which activity in one part of the receptive field is spread to the rest of the receptive field, influencing even regions that have not been stimulated. This corresponds to the spreading of activity across the cortical surface. Activity is distributed not just between discrete receptive-field regions but continuously throughout the receptive field, allowing interactions to occur even within subfields. The actual shape of such an interaction so far has not been measured experimentally; we assume that it falls off exponentially with distance because this form is computationally simple. A point (x', y') adds to the activity of the point (x, y) an amount proportional to

$$F(x - x', y - y') = \exp\left(-\frac{\sqrt{(x - x')^2 + (y - y')^2}}{\lambda}\right) \quad (3)$$

The above expression for the activity distribution mechanism is convolved with the spatial structure $g(x, y)$ of the cortical receptive field to yield the activity of the middle layer of cells in Fig. 1

$$B(x, y, t) = \iint g(x', y')C(x', y', t)F(x - x', y - y')dx'dy' \quad (4)$$

These cells have oriented receptive fields. In fact, for static or flashing stimuli the spatial structure of their receptive fields is given by

$$B(x, y) = g * F = \iint g(x', y')F(x - x', y - y')dx'dy' \quad (5)$$

which is similar to a Gabor function.

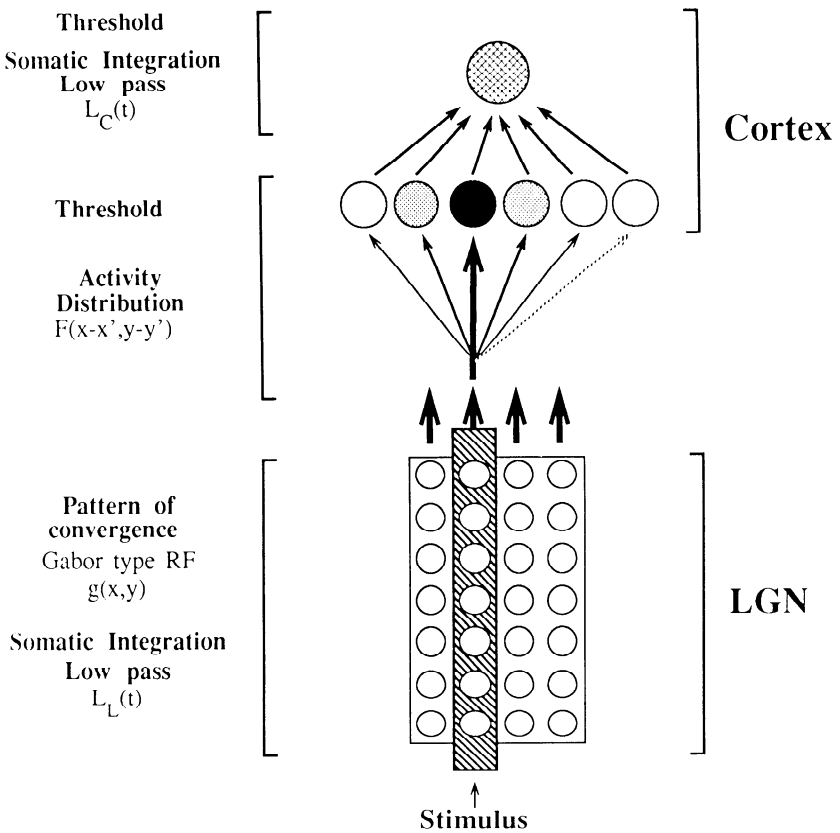

FIG. 1. Schematic of the model. Basic stages (reflected in the equations) are represented by sub- and intracortical processing of the visual signals. LGN cells act as low-pass filters (*Eq. 2*). The pattern of convergence determines the spatial structure of the receptive field (the Gabor function). Distribution of activity, $F(x - x', y - y')$, occurs intracortically through threshold units (circles); their activity is given by $B(x, y, t)$ (*Eq. 4*). Finally there is a second low-pass filter and threshold in the topmost cortical cell (*Eqs. 6* and *7*).

In addition, these units behave like velocity low-pass cells. The "charging curve" for a low-pass filter is shown in Fig. 2*A*; the longer there is positive input, the larger the filtered response becomes. Because a faster moving stimulus stays in the receptive field for less time, the unit will respond less. In other words, it is like a velocity low-pass cell. This effect can be shown in a diagram by drawing the receptive field with a smaller peak height for higher velocities.

Low-pass filtering also results in a directional bias (Fig. 2*B*). In a low-pass filtered unit any given value of activity will not be reached instantaneously but delayed according to the slope of the response curve (Fig. 2*A*). Thus a stimulus traveling from right to left (Fig. 2*B*, *bottom*) will lead to inhibition that reduces the peak response in the excitatory region for some time. Similarly, a bar moving in the opposite direction (Fig. 2*B*, *top*) will excite the positive region, reducing the amplitude of the negative peak. However, this

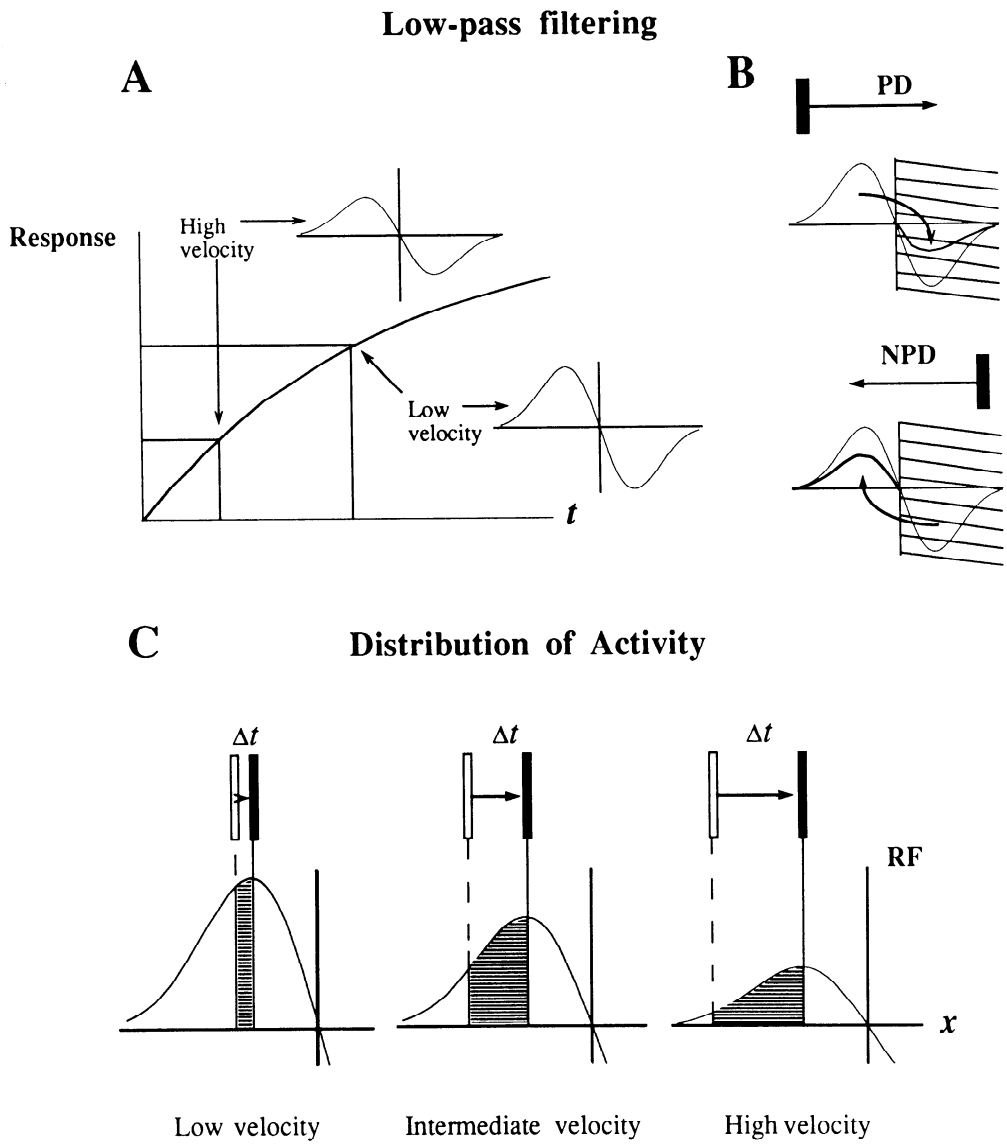

FIG. 2. Simplified representation of the behavior produced by the model. *A*: effect of low-pass filtering. Response of a cell at the time when bar leaves its receptive field is plotted against amount of time the bar was in the receptive field. Faster moving bars remain in the receptive field of a particular cell for less time. The cell's activity increases with time, because of low-pass filtering as shown; consequently a shorter exposure to the stimulus results in a lower activity. Therefore the peak response of cells to faster bars is less, i.e., they display velocity low-pass behavior. This can be visualized by drawing receptive fields with decreasing peak heights at increasing stimulus velocities. *B*: low-pass filtering results in direction tuning because the response in the nonpreferred direction is reduced due to inhibition carried over from the negative region. *C*: effect of distributing the activity from low-pass filtered cells. Maximum response of a cell to a moving stimulus occurs approximately at the receptive field peak (black bars). As shown above the effect of low-pass filtering at different stimulus velocities can be thought of as if the receptive-field peak height was changing. For a fixed time interval Δt, the stimulus moves a longer distance in the receptive field at a higher velocity (shaded areas). The activity distribution mechanism results in an accumulation of activity corresponding to the area of the shaded regions. The width of those regions is larger for higher velocities, but the peak height is smaller; thus these two opposing mechanisms lead to a maximal response at an intermediate velocity and thus to velocity-tuned behavior.

reduction has no effect on the cell activity because cell's responses are rectified (represented by the hatched area), so they cannot have negative impulse rates. Thus first-layer cortical units act according to the synergy model for direction selectivity (Hubel and Wiesel 1962).

We assume that activity distribution occurs only from regions that are stimulated strongly enough because we postulate thresholding in the first layer of cortical cells. We therefore define the inputs to the top level cell in Fig. 1 by

$$B_{T_1} = \begin{cases} B(t) - T_1 & \text{if} \quad B(t) > T_1 \\ 0 & \text{otherwise} \end{cases}$$

Up to *Eq. 4* our system is space-time separable and linear. Introducing a threshold makes it nonseparable and nonlinear. Note, however, that the response still is separable for subthreshold input (B_{T_1} is zero) and separable for large suprathreshold input (B_{T_1} is the same as B in *Eq. 4* except for a subtracted constant).

Figure 2*C* shows a simplified diagram of the effect of the distribution of activity. For a given time interval Δt activity is accumulated over wider areas of the receptive field for different sweeps starting at higher stimulus velocities (shaded areas). For this reason, increasing the stimulus velocity at low speeds will result in an increased response. At a certain velocity, however, an optimum is reached, because low-pass filtering decreases the height of the shaded area (Fig. 2*A*) more rapidly than the width of the shaded area increases at high enough velocities. Therefore the cortical cell has its maximum response at some intermediate velocity (velocity-tuned cell).

The cortical cell being studied (the *top cell* in Fig. 1) is assumed to behave like another first-order low-pass filter, i.e., $L_C(t') = e^{-t'/\tau_C}/\tau_C$. So then the activity of the cell is the filtered sum of its inputs B_{T_1}

$$A(t) = \int_0^t \iint L_C(t') B_{T_1}(x, y, t - t') dx dy dt' \tag{6}$$

Finally we implemented another threshold in the cortical cell

$$A_{T_2}(t) = \begin{cases} A(t) - T_2 & \text{if} \quad A(t) > T_2 \\ 0 & \text{otherwise} \end{cases} \tag{7}$$

For bars moving at an angle θ with the x axis, *Eq. 1* can be modified by substituting x_θ for x

$$x_\theta = x \cos\theta + y \sin\theta$$
$$y_\theta = -x \sin\theta + y \cos\theta \tag{8}$$

The complete form (*Eq. 7*) is computationally expensive because it has four integrals over space and two over time. In the next section we introduce several assumptions and approximations that lead to a simpler, computationally faster form of *Eq. 7*.

APPROXIMATIONS. First we assume that only regions (i.e., first layer cortical cells) underneath the bar will be excited enough to contribute to the mechanism of activity distribution because of the threshold T_1. As a result, we only have to integrate over the region of the bar in *Eq. 6*

$$A(t) = \int_0^t \iint_{(x,y)\in \text{bar}} L_C(t') B(x, y, t - t') dx dy dt' \tag{9}$$

Second, we assume that the bar is narrow and moves at constant velocity. The input to the system $I(x, y, t)$ can then be approximated by a δ-function

$$I(x, y, t) = \begin{cases} \delta(x - vt) & \text{if} \quad -b_l/2 < y < b_l/2 \\ 0 & \text{otherwise} \end{cases} \tag{10}$$

where b_l is the length of the bar. This changes *Eq. 2* into

$$C(x, y, t) = \begin{cases} \exp\left(\dfrac{x - vt}{v\tau_L}\right) & \text{if} \quad x < vt \text{ and } \quad b_l/2 < y < b_l/2 \\ 0 & \text{otherwise} \end{cases} \tag{11}$$

We do not need to integrate $C(x, y, t)$ over regions where it is zero, so *Eq. 4* becomes

$$B(x, y, t) = \int_{-\infty}^{vt} \int_{-b_l/2}^{b_l/2} g(x', y') C(x', y', t) F(x - x', y - y') dx' dy' \tag{12}$$

Also, integrating over the area of a δ-function bar eliminates the integral over bar width (x), and *Eq. 9* changes to

$$A(t) = \int_0^t \int_{-b_l/2}^{b_l/2} L_C(t') B(vt, y, t - t') dy dt' \tag{13}$$

Finally, we assume that distribution of activity is significant only when it is in the direction of motion. Activity distributed in other directions must traverse a longer distance to reach the region under the bar and is consequently less effective. Therefore $F(x - x', y - y')$ can be replaced by

$$\exp\left(-\frac{|x - x'|}{\lambda}\right)$$

Thus $B(x, y, t)$ is independent of y. This approximation was tested with a number of different parameter sets and found to result in no qualitatively different behavior.

The effect of the last approximation is that *Eq. 13* is replaced by

$$A(t) = \int_0^\infty \int_{-\infty}^{vt'} \int_{-b_l/2}^{b_l/2} g(x', y') L_L\left(t - t' - \frac{x'}{v}\right) \times F[v(t - t') - x'] dy' dx' dt' \tag{14}$$

T_2 is then subtracted from $A(t)$ as in *Eq. 7*.

Compared to *Eq. 6*, *Eq. 14* contains only three integrals and was used for all the simulations presented here.

PARAMETER RANGES. Although this simulation reproduced findings in several experimental animals, parameters appropriate for area 17 of the adult cat were chosen. Receptive-field shape parameters in general were adjusted to reliably measured values from receptive fields of simple cells (Jones and Palmer 1987a). We found that setting τ_L and τ_C to different values did not result in qualitatively different behavior. This is to be expected because the two low-pass filters $L_L(t)$ and $L_C(t)$ can be combined into a single low-pass filter of higher order. Therefore, throughout all simulations, τ_L and τ_C were identical. A reasonable range for τ is 0–80 spanning the low-pass behavior range found experimentally with drifting gratings (Ikeda and Wright 1975a). This is not the time constant of the membrane, which typically is on the order of 20 ms (see DISCUSSION).

It is more difficult to determine the range for λ. Short-range interactions have been reported at distances <0.30° in the visual field (Ganz and Felder 1984). However, there are indications that interactions span as much as 5° (Duysens 1987; Jones 1970). We used a range of 0–2° for λ.

METHODS

Data presentation

Most of the figures include three-dimensional plots of the Gabor function that represent the shape of the receptive field. Orientation tuning curves are displayed as polar plots. The peak response (the maximum value of A_{T_2}) for a given direction of motion is shown as a vector in a polar coordinate diagram. Because the experimental data were recorded in 30° steps, the same step size is also used in the simulations. Because of the lack of noise, a finer step size does not affect any of the results reported here. All polar plots are normalized with respect to their peak value.

Experimental procedures

A complete review of the real data that were used to compare to simulation results is found in Orban (1984). A few previously unpublished results presented here were obtained in extracellular recordings from area 17 of the paralyzed and anesthetized cat. These data were measured during the experiments reported by Wörgötter and Eysel (1989). Experimental procedures are described in detail in that paper.

RESULTS

Figure 3 shows typical examples of polar plots obtained with the model for moving bars (Fig. 3, *C* and *D*) and flashing bars (Fig. 3, *E* and *F*). The spatial parameters of the Gabor functions (Fig. 3, *A* and *B*) are for an "average" cortical simple cell with an excitatory zone width of ~1° (Jones and Palmer 1987a). Histograms for a bar moving along the preferred axis of motion (insets in Fig. 3, *C* and *D*) show that the temporal response profile looks similar to that of cortical cells. The spatiotemporal mechanisms included in the simulation (τ = 80 ms, λ = 0.4°) lead to a directionally tuned behavior for the odd-shaped receptive field (Fig. 3*D*) as explained in Fig. 2*B*. The orientational component is approximately the same for moving and stationary flashing bar (Fig. 3*F*).

Velocity low-pass cells

Cells generally act as low-pass filters, but the importance of distributing activity is unclear, and this mechanism need not necessarily be a feature of all cells. Figure 4 shows the response of the cell in Fig. 3*B* without the activity distribution mechanism. τ was set to 80 ms on the *left* and, to show a limit case, to the very low value of 1 ms on the *right*.

The velocity tuning curve (Fig. 4*B*) shows the expected velocity low-pass behavior (see Fig. 2*A*) with a −3-dB point (68% of maximum) of ~5°/s. The velocity response curve is similar to curves from real velocity low-pass cells (*inset* in Fig. 4*B*).

The velocity tuning curve corresponding to small τ is flat for low to moderate velocities (Fig. 4*D*), resembling that of a velocity broadband cell. Only at very high velocities is the activity reduced significantly; the −3-dB point is >100°/s. For comparison, tuning curves from real velocity broadband cells are shown in the *inset* of Fig. 4*D*.

Figure 5 shows the effect of varying τ and σ_x on the velocity tuning curves of the velocity low-pass and broadband cells in Fig. 4. Increasing τ strengthens the velocity low-pass

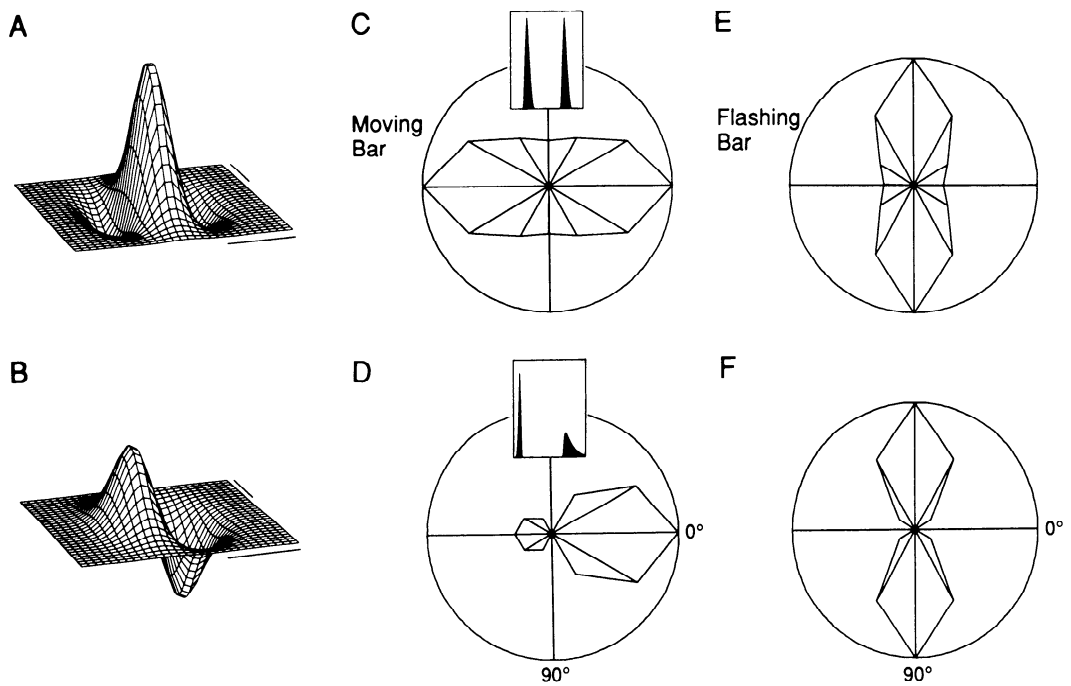

FIG. 3. Typical simulated cell behavior. Each row represents 1 cell. *A* and *B*: Gabor functions that were used to model the spatial receptive-field structure. Parameters: σ_x = 0.4°, σ_y = 0.5°. *A*: f_0 = 0.61/°. *B*: f_0 = 0.4/°. Scale bars: 1°. *C* and *D*: tuning curves for moving bars. Parameters: τ = 80 ms, λ = 0.4°, b_l = 10°. *C*: v = 3.84°/s. *D*: v = 25°/s. Insets: histograms for a forward and backward sweep in the preferred direction. *E* and *F*: polar plots for stationary flashed bars centered at the peak of the largest excitatory region.

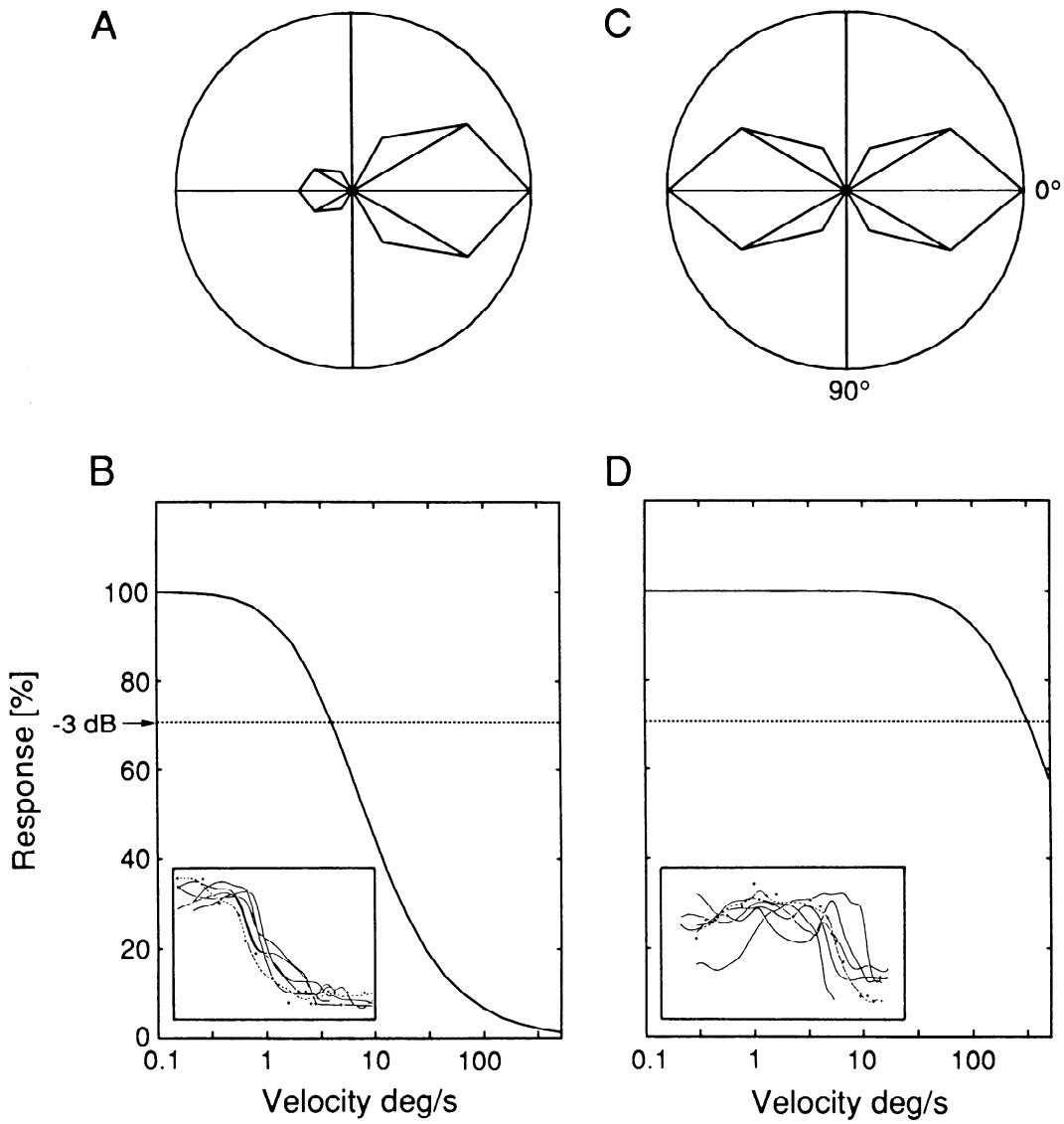

FIG. 4. Results from the model with only low-pass filtering. Simulations of both velocity low-pass (*left*) and velocity broadband (*right*) cells are shown. The velocity low-pass cell was generated with the same parameters as Fig. 3, *B* and *D* (σ_x = 0.4°, σ_y = 0.5°, f_0 = 0.408/°, τ = 80 ms, λ = 0.4°, b_l = 10°; v = 25°/s); the parameters of the broadband cell were the same except that τ = 1 ms. *A* and *B*: tuning curves for v = 25°/s. *C* and *D*: velocity tuning curves. *Insets*: (modified from Orban 1984, Fig. 8/5) typical recorded velocity low-pass and broadband behavior. Response is shown as a percentage of the largest value on the particular velocity tuning curve.

behavior (Fig. 5, *A* and *B*) because increasing τ is like shifting the curve in Fig. 2*A* to the right. Changing σ_x is equivalent to changing the size of the cortical cell's receptive field. A moving bar remains longer in a larger receptive field, causing the cortical cell to respond more at all velocities. However, because the curve in Fig. 2*A* is nonlinear, this effect is especially pronounced for high velocities. Therefore the result in a rightward shift of the velocity tuning curve, as can be seen in Fig. 5, *C* and *D*. This result reflects findings that cells with wider receptive fields respond more strongly to higher velocities (Baker 1988; Baker and Cynader 1986; Orban et al. 1981a).

Velocity-tuned cells

Velocity-tuned cells have a velocity tuning curve with a distinct maximum. The low-pass and activity distribution mechanisms together produce velocity-tuned behavior in the cortical cells, as explained in Fig. 2*C*. However, with odd Gabor functions the simulated cells show neither the strong direction selectivity nor the stability of direction preference to contrast reversal, which most velocity-tuned cells have. An odd receptive field produces exactly the same response to a light bar moving in the preferred direction and a dark bar moving in the opposite direction because the heights of the largest positive and negative peaks of the Gabor functions are equal. Therefore without additional mechanisms the preferred directions for light and dark bars will be opposite.

However, it has been shown that few simple-cell receptive fields have exactly even or odd symmetry; in fact, values of ϕ (the phase shift in *Eq. 1*) are spread out fairly uniformly over possible values (Field and Tolhurst 1986; Jones and Palmer 1987a). An asymmetric receptive field

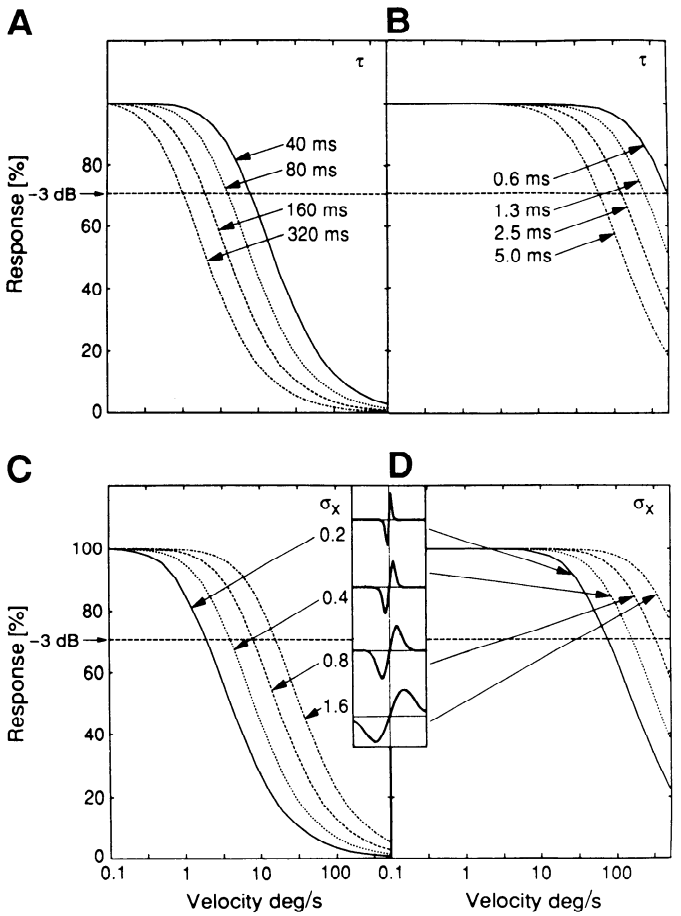

FIG. 5. Effect of parameter values on the model. Parameters that were not varied are the same as in Fig. 3, *B* and *D* ($\sigma_x = 0.4°$, $\sigma_y = 0.5°$, $f_0 = 0.408/°$, $\tau = 80$ ms, $\lambda = 0.4°$, $b_l = 10°$; $v = 25°/s$). *A* and *B*: τ variations. *C* and *D*: receptive-field size variations. The product $\sigma_x f_0$ was kept constant at 0.16 so that only the scale of the receptive field changed.

will not respond equally to dark and light bars moving in opposite directions because the largest positive and negative peak heights are not equal. Consequently, the threshold of the cortical cell can be set to eliminate the response to the less effective stimulus. As a result, the cell will still respond strongly to one contrast and not at all to the other. This corresponds to the behavior of the velocity-tuned directional selective DS_1 cells (Ganz and Felder 1984). Obviously DS_1 cells are an extreme case; by adjusting the threshold any intermediate response to bars of reversed contrast can be obtained.

Velocity tuning curves for light and dark bars moving in their preferred directions are shown for such a cell in Fig. 6*C*. This cell responds most strongly to a light bar moving rightward. The histogram in the *inset* (Fig. 6*B*) demonstrates that thresholding, as expected, does not significantly affect the temporal pattern of the response. The mean direction index (MDI[2]) averaged over all velocities is 66.9; the parameters in this simulation have been set for the lower limit case ($MDI > 66$), which qualifies a cell as direction selective (DS type) (see also Orban 1984). This case was chosen so that the cell shows pronounced response to a light bar and still has a perceptible response to a dark bar. It is no problem to eliminate the remaining response to a dark bar completely by changing the phase shift (ϕ) or the threshold. Also, changes in the parameter set can be made to raise the

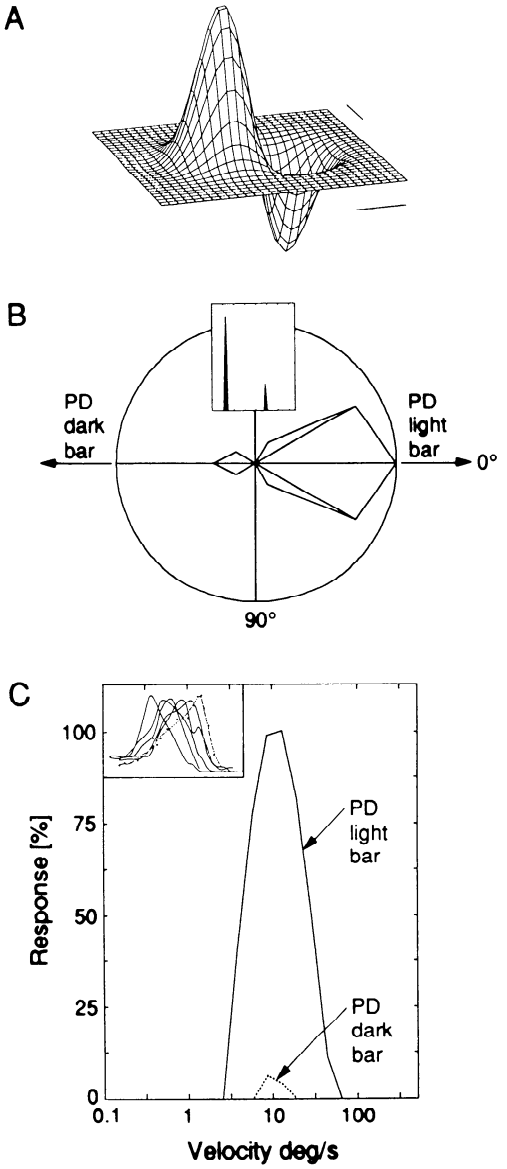

FIG. 6. Velocity-tuned DS cells can be generated with a phase-shifted Gabor function with a threshold. *A*: the Gabor function used. Deviation from odd symmetry is hardly perceivable. Parameters used: $\sigma_x = 0.8°$, $\sigma_y = 0.5°$, $\phi = 19°$, $f_0 = 0.255/°$. Scale bars are 1°. *B*: polar plot for a bar moving at 13°/s (optimal velocity). $\tau = 80$ ms, $\lambda = 2.0°$, $b_l = 10°$. The threshold used was 0.6 of the response to a light bar moving in the preferred direction at the optimal velocity. This cell has a mean direction selectivity index of 66.9. The histogram for a light bar moving along the axis of preferred motion at the optimal velocity is shown. *C*: velocity tuning curves for a dark and a light bar. Note that the preferred directions for dark and light bars are opposite. Any dark bar response of such a small amplitude will be lost in noise (maintained discharge) in a physiological experiment. *Inset*: (modified from Orban 1984, Fig. 8/5) typical velocity-tuned behavior of real cortical cells.

[2] The direction index DI is defined as $DI = 100[(IR_{PD} - IR_{NPD})/IR_{PD}]$ with IR_{PD} the peak impulse rate in the preferred direction and IR_{NPD} the peak impulse rate in the nonpreferred direction. The mean direction index MDI is defined as $MDI = \sum_i IR_{PD_i} DI_i / \sum_i IR_{PD_i}$ summing the values over all tested velocities i (Orban 1984).

MDI to values close to 100. However, there is a trade-off between the strength of direction selectivity and the response strength for the nonoptimal contrast: decreasing ϕ increases direction selectivity but also increases the response to the nonoptimal contrast.

Figure 7 shows the effect of parameter variation on the velocity tuning of the cell from Fig. 6. For the same reasons as for velocity low-pass cells (Fig. 4), increasing τ lowers the optimal velocity (Fig. 7*A*), and increasing σ_x raises the optimal velocity (Fig. 7*C*). *Insets* show cross sections of the receptive fields for the various values of σ_x. Larger values of λ result in higher optimal velocities (Fig. 7*B*). This is in agreement with experimental findings that show that a longer range spatial interaction leads to a higher optimal velocity (Baker 1988; Mikami et al. 1986). The phase shift ϕ has essentially no effect on velocity tuning (Fig. 7*D*). *Insets* show cross sections of the receptive fields for various values of ϕ.

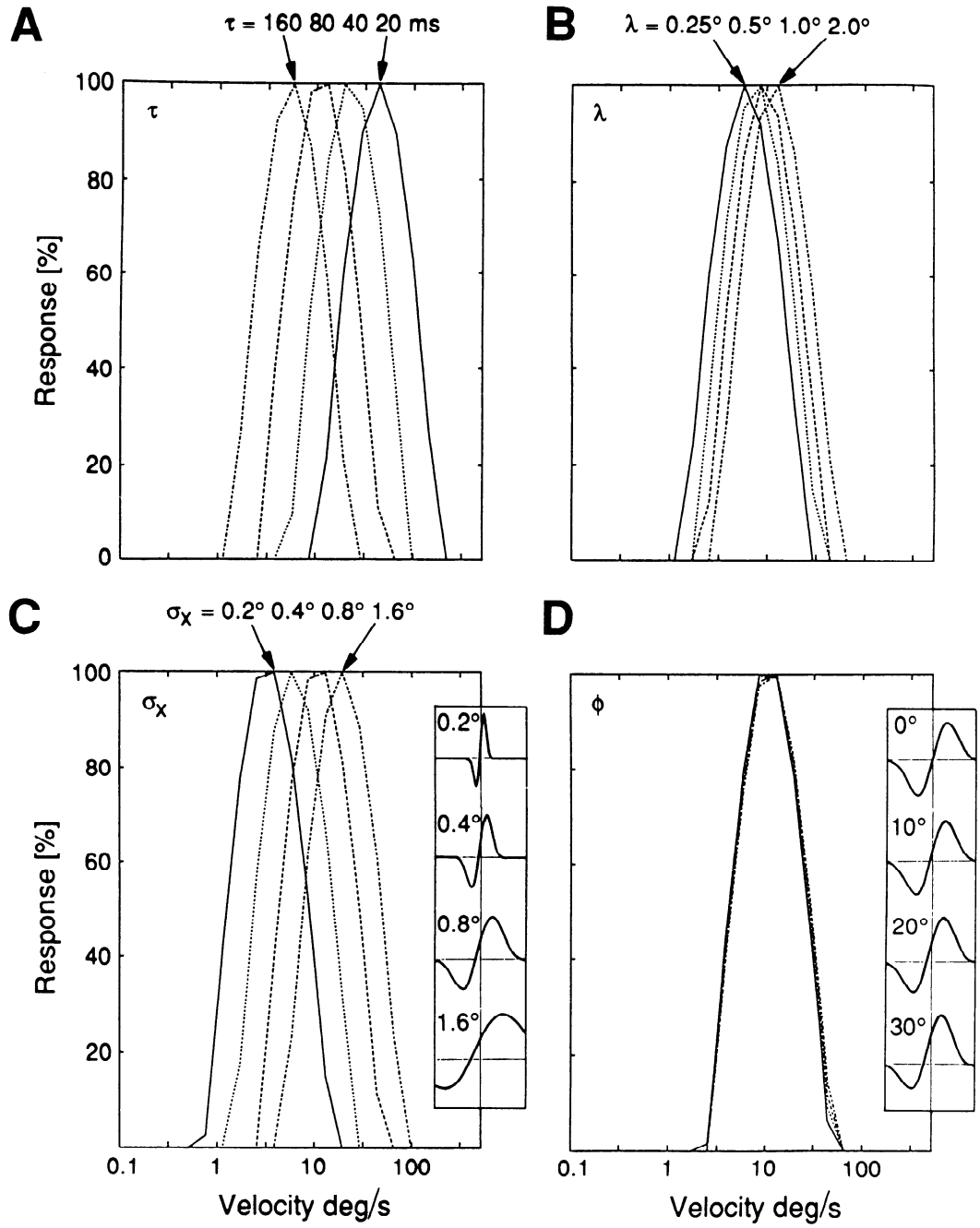

FIG. 7. Effect of various parameters on the velocity tuning of the cell in Fig. 6. Basic parameter set: $\sigma_x = 0.8°$, $\sigma_y = 0.5°$, $f_0 = 0.255/°$, $\tau = 80$ ms, $\lambda = 2.0°$, $b_l = 10°$, $\phi = 19°$. The threshold used was 0.6 of the response to a light bar moving in the preferred direction at the optimal velocity. *A*: variations of τ. *B*: variations of λ. *C*: variations of receptive-field size (holding $\sigma_x f_0$ constant at 0.2 so only the scale of the receptive field changes). Plots to the *right* are cross sections of Gabor functions through the x-axis. *D*: variations of phase shift. Small plots to the *right* are cross sections of the Gabor functions through the x-axis, demonstrating how changes in σ_x or ϕ affect the shape of the receptive field.

Responses to moving dots

Recently Wörgötter and Eysel (1989) reported that the strongest response to a small moving dot in most cortical cells is obtained when the dot moves along the long axis of the receptive field. Figure 8, *A* and *B*, shows a result from this study that is reproduced in the simulation (Fig. 8, *C* and *D*). Such responses are not surprising if the receptive field is analyzed according to the model. A dot can remain entirely within the excitatory region of the receptive field if it moves vertically, so no inhibition is ever seen by the cortical cell. A bar, however, must be rotated by 90° to cover the excitatory zone of the receptive field optimally. The Gabor receptive field is small and odd symmetrical (Fig. 8*E*). This corresponds roughly to the shape of the real receptive field shown in Fig. 1 in Wörgötter and Eysel (1989), although a small and weak off-excited region was found in the real cell on the right side of the receptive-field center.

In several cortical cells a superposition of the axial response and the orthogonal response to a bar was observed (Fig. 9, *A* and *D*) during stimulation with a short bar (bar length, between 0.5 and 1.5°). Nondirection-selective (NDS) cells with this type of behavior produce a four-lobed polar plot (Fig. 9*A*). The same behavior can be obtained (Fig. 9*B*) with an even, wide Gabor function (Fig. 9*C*). This corresponds to the basic shape of the real receptive field as measured by hand plotting (not shown). The rather unusual shape of the receptive field in such cells was, in most cases, accompanied with an indistinct separation between ON- and OFF-zones, which made it difficult to classify the cells as clearly simple or complex.

For some DS cells (e.g., Fig. 9*D*) the dot response may be a bilobed polar plot with some residual direction selectivity along the preferred axis of motion for a bar (0° axis, in this case) (compare with Fig. 3*A* in Wörgötter and Eysel 1989). The model shows this direction-selective behavior for a dot (Fig. 9*E*). An odd Gabor function (Fig. 9*F*) was used, which is similar to the real field (see Fig. 3*B* in Wörgötter and Eysel 1989). A similar but less pronounced behavior can already be seen in Fig. 8, *B* and *D*.

Previous investigators (Henry et al. 1974a,b) reported that the preferred axis of motion for a dot is the same as for the bar and that the dot has a wider polar plot, i.e., a reduced tuning strength. This disagrees with the findings of Wörgötter and Eysel (1989). The discrepancy between the studies can probably be explained by the large dot size that Henry et al. (1974a) used (diameter >0.4°). Also the stimu-

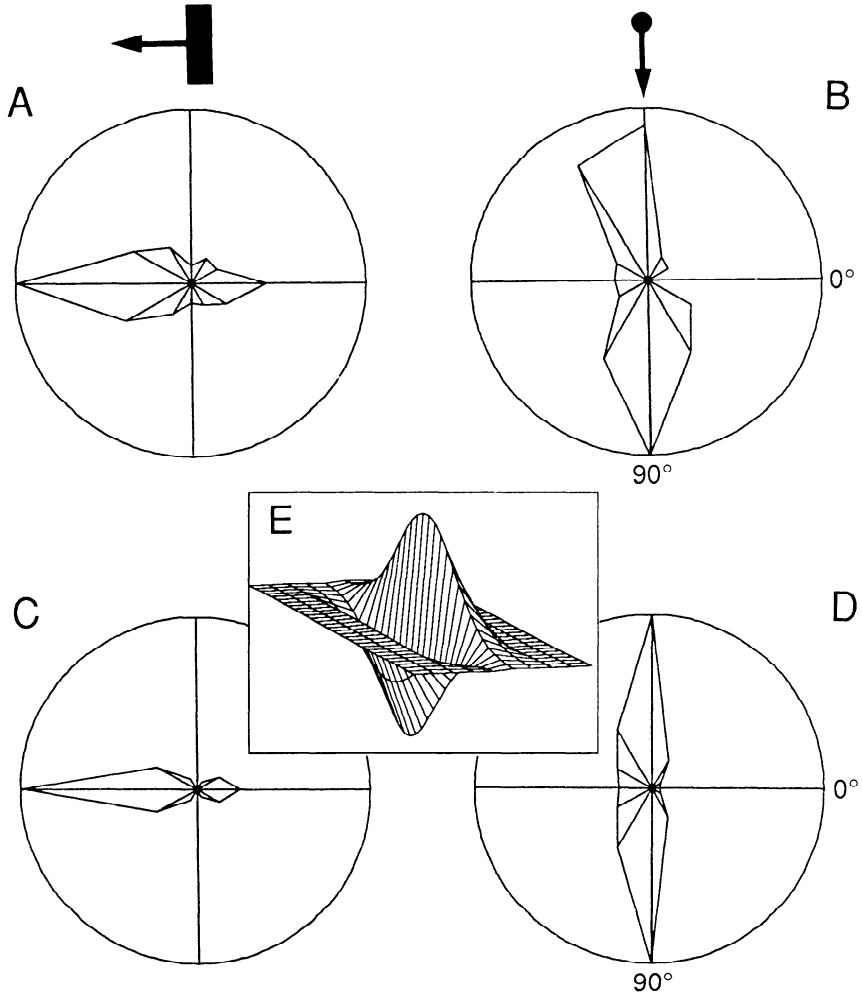

FIG. 8. Recorded and simulated responses to bars and dots. Note that the axis of preferred motion for a dot is shifted 90° from that of a bar. *A* and *B*: (modified from Fig. 1, *B* and *C* in Wörgötter and Eysel 1989) polar plots for moving a moving bar/dot recorded from a simple cell in cat area 17. *C* and *D*: polar plots showing the response of the model to a moving bar or dot. Parameters: σ_x = 0.1°, σ_y = 0.5°, f_0 = 2/°, τ = 35 ms, λ = 0.15°. The dot was modeled as a very short bar (length, 0.1°). Response to a dot is ~½ as large as the response to a bar. *E*: Gabor function used to model the spatial receptive field.

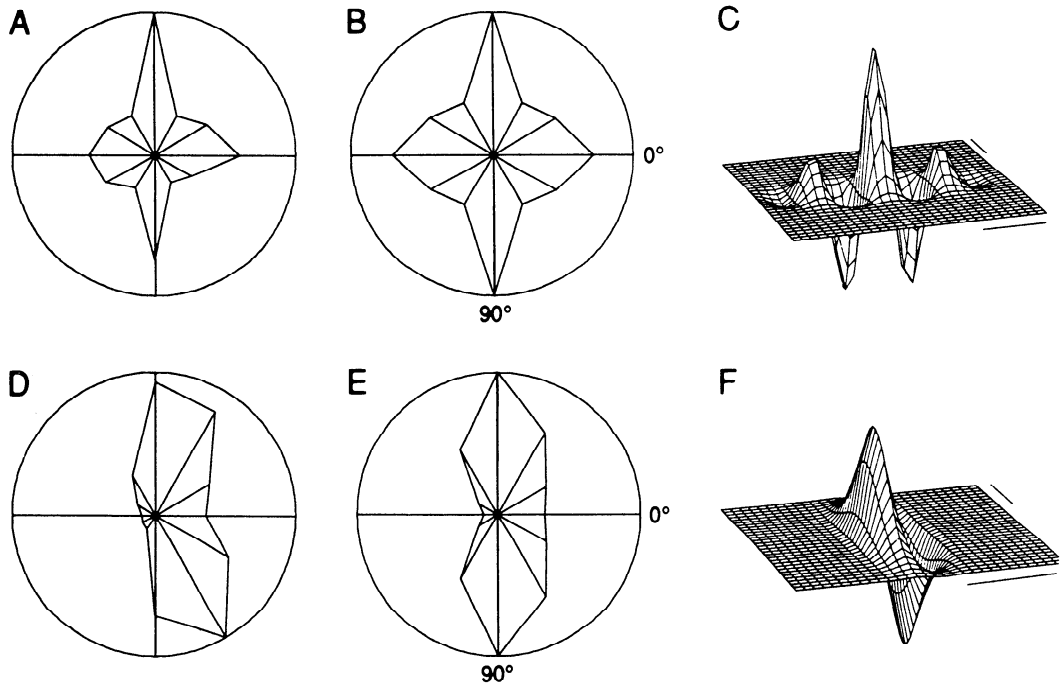

FIG. 9. The model can account for some other unusual polar plots for moving bars that have been observed. *A*: a recorded polar plot for a moving bar of intermediate length (4.1°) (F. Wörgötter and U. T. Eysel, unpublished data). *B*: polar plot for a moving bar generated by the model. Parameters: $\sigma_x = 0.6°$, $\sigma_y = 0.23°$, $f_0 = 1.0/°$, $\tau = 200$ ms, $\lambda = 0.9°$, $v = 11.5°/s$, $b_l = 0.95°$. *C*: the Gabor function used. Scale bar is 1°. *D* and *E*: polar plot of a simple cell's response to a moving dot (modified from Fig. 3*A* in Wörgötter and Eysel 1989) and a simulation of it. Parameters used in *E* were $\sigma_x = 0.2°$, $\sigma_y = 0.5°$, $f_0 = 1.0/°$, $\tau = 100$ ms, $\lambda = 0.4°$, $v = 8.0°/s$, $b_l = 0.1°$. *F*: the Gabor function used to generate the results in *E*. Scale bar is 1°.

lus may have been misaligned with respect to the receptive-field center (see Fig. 4 in Wörgötter and Eysel 1989). Under these conditions our model reproduces the results of Henry et al.

Figure 10 shows simulations using an even Gabor receptive field and an offset stimulus that was centered on X in Fig. 10*A* similar to the offset used by Wörgötter and Eysel (Fig. 4 in Wörgötter and Eysel 1989). The response to the long bar (length, 10°) is normal (Fig. 10*B*) because the bar is much longer than the receptive field. The tuning strength is reduced for shorter bars, whereas the preferred axis of motion remains the same (Fig. 10, *C* and *D*), corresponding to the findings of Henry et al. (1974a). The dot size used to compute the dot response (Fig. 10*E*) is much smaller (diameter, 0.1°) than all dot sizes used by Henry et al. Thus the preferred axis of motion for the dot is now different from that for the bar.

In contrast to the examples with correct stimulus alignment (Figs. 8 and 9), in this case the preferred axis of motion for the dot is tilted <90° to that of the bar. A properly aligned dot always moves along the ridge of the Gabor function when it moves vertically; a misaligned dot, on the other hand, can produce a larger response if it moves at a slight angle from the vertical, because then it will cross the ridge. In the report Wörgötter and Eysel (1989) found this behavior in ~30% of the cells. Our model suggests that this was caused by a small misalignment between the receptive-field center and the center of rotation of the stimulus.

Predictions

VELOCITY TUNING FOR DOT STIMULI. Velocity tuning curves for a simulated velocity low-pass and a velocity-tuned cell in response to bars and dots are shown in Fig. 11*B* for the Gabor receptive field in Fig. 11*A*. Velocity tuning for the bar is measured conventionally along the preferred direction and for the dot at right angles to that. The velocity tuning curves for dot simulation are shifted to higher velocities than for a bar. This effect can be expected because the response to different velocities is influenced by the receptive-field size. In the horizontal direction the width of the receptive field is determined by the spatial period, $1/f_0$. In the vertical direction the effective width (i.e., length) depends only on σ_y. As shown above (see Figs. 5 and 7), cells with wider receptive fields have a higher response at larger velocities. Consequently, the response along the long axis has a higher optimal velocity than the response across.

ORIENTATION TUNING AT NONOPTIMAL VELOCITIES FOR BAR AND DOT STIMULI. From the above result (Fig. 11) one would also expect that the polar plot of a cell might be different at different velocities because the velocity tuning curves of stimuli moving in different directions are different. For the receptive field shown in Fig. 11*A*, the response to a bar moving in the vertical direction decreases less than the response in the horizontal direction (see above), so the tuning curve for a bar should be broader at high velocities. Figure 12, *A–E*, show this result for a velocity-tuned cell.

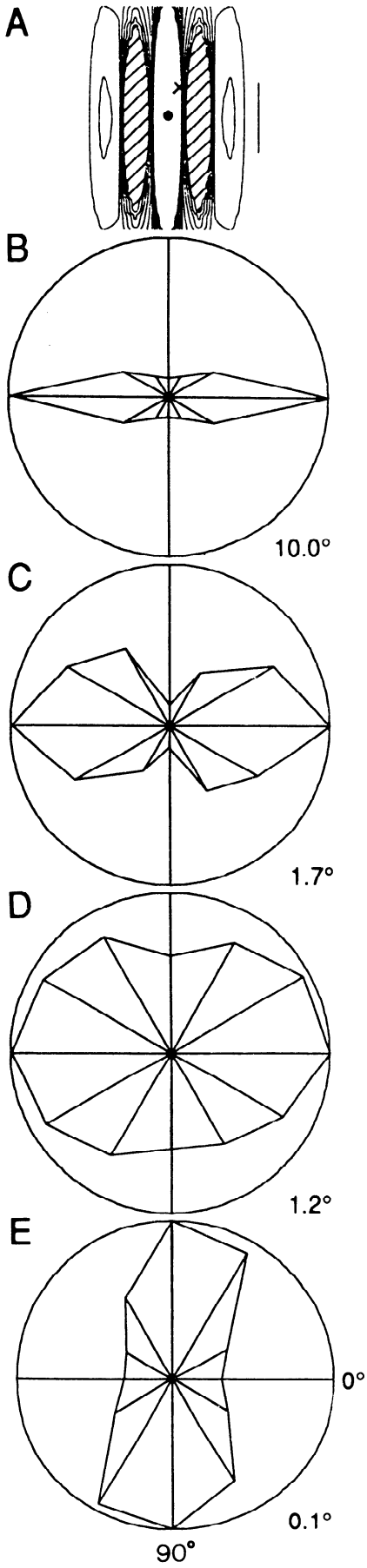

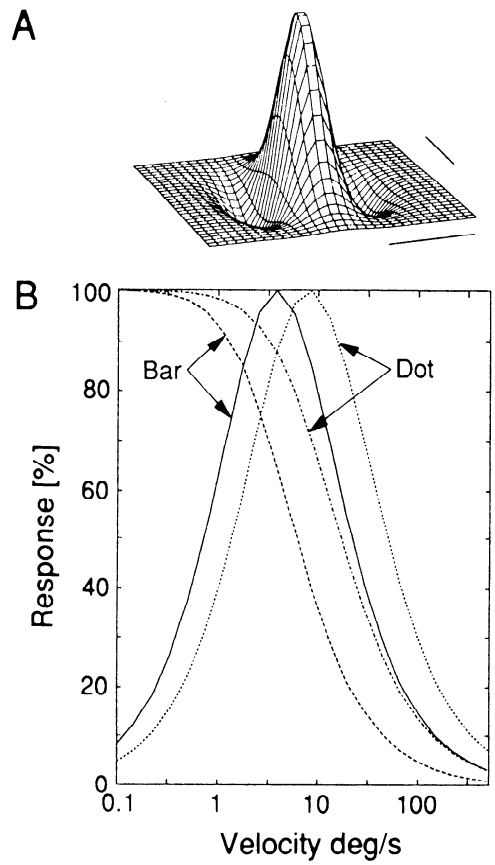

FIG. 11. Optimal velocity for a dot is always higher than for a bar. All parameters are the same as in Fig. 3*A* ($\sigma_x = 0.4°$, $\sigma_y = 0.5°$, $f_0 = 0.613/°$, $\tau = 80$ ms, $\lambda = 0.4°$, $b_l = 10°$). *A*: the Gabor function. Scale bar is 1°. *B*: velocity tuning curves for bars and dots moving along their respective optimal axes of stimulation for a simulated velocity low-pass and velocity-tuned cell.

Velocity is increased in four steps starting at 0.1°/s, including the optimal velocity 2.5°/s (Fig. 12*C*). Scale bars underneath the polar plots show the response strength relative to the optimal response. A similar, although much less pronounced, effect occurs for a velocity low-pass cell. In these cells for the highest velocities tested the tuning is reduced to an extent similar to that shown in Fig. 12*D*.

The reverse effect—sharpening of tuning with increasing velocity—arises for the moving dot (Fig. 12, *F–J*). The optimal velocity for the dot (15°/s) is higher than that for the bar and falls in between Fig. 12, *H* and *I*.

FIG. 10. If the bar is not passed exactly over the center of the receptive field, the axis of preferred motion for a dot will not be rotated 90° relative to that of a bar. *A*: contour plot of the Gabor function used. Areas where the Gabor function is negative are hatched. The center of the function is marked by a dot; the bar's center of rotation is marked by the X, which corresponds to a shift of 0.17° in the x direction and 0.4° in the y direction. Parameters: $\sigma_x = 0.4°$, $\sigma_y = 0.9°$, $f_0 = 1.0/°$, $\tau = 80$ ms, $\lambda = 0.8°$, $v = 8.0°/s$. Scale bar is 1°. *B–E*: for shorter bars a widening of the polar plot is observed until for a very short bar (i.e., dot) the axis of preferred motion is shifted 90° away from that of a long bar. Relative response amplitudes (from *top* to *bottom*) are 1, 0.6, 0.46, and 0.15.

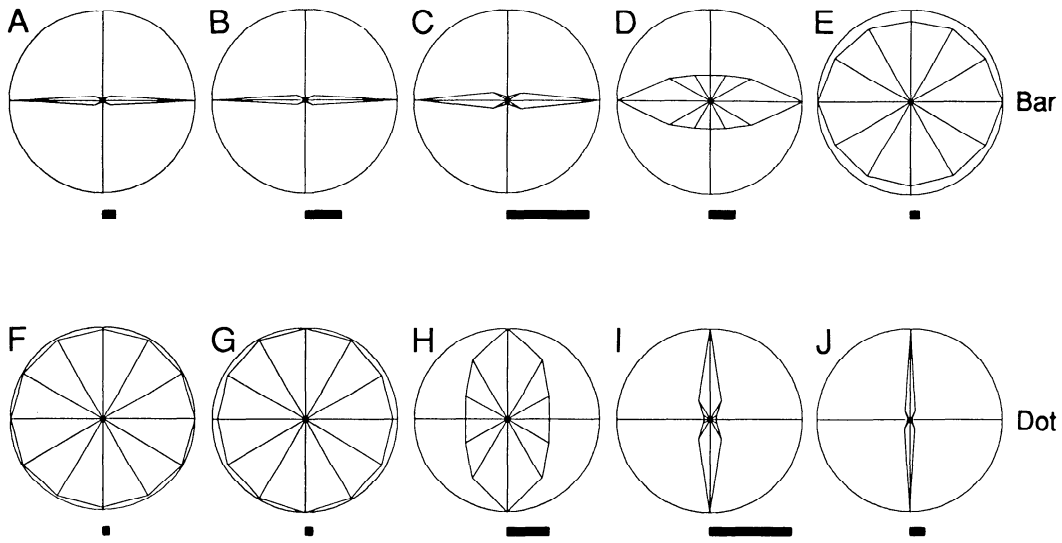

FIG. 12. Polar plots for bars and dots moving at various velocities. As velocity increases the tuning sharpens for a dot and widens for a bar. All parameters are the same as in Fig. 10 ($\sigma_x = 0.4°$, $\sigma_y = 0.9°$, $f_0 = 1.0/°$, $\tau = 80$ ms, $\lambda = 0.8°$). Velocities used (from *left* to *right*): 0.1, 0.5, 2.5 (optimal velocity for a bar), 20, and 500°/s. Scale bars below the figures indicate the relative amplitude of the response. Amplitude of the dot response is much smaller than that of a bar at the same velocity. For purposes of comparison, it has been scaled up by a factor of 4.

DISCUSSION

Many aspects of simple cell behavior can be explained by LN models, and the use of Gabor functions to describe a receptive field has been very successful in predicting the response to stationary (i.e., flashing or counter-phasing) stimuli (Daugman 1980, 1984; Jones and Palmer 1987b; Kulikowski et al. 1982; Marčelja 1980). Static stimuli, however, ignore temporal effects, which also characterize a cortical cell. Therefore, in our model, Gabor functions are supplemented with neurobiologically plausible spatiotemporal mechanisms. We combine the low-pass behavior of the cells (Ikeda and Wright 1975a; Movshon et al. 1978c) and the mechanism of distributing the activity (Bishop et al. 1971; Emerson and Gerstein 1977b; Eysel et al. 1987, 1988; Goodwin and Henry 1975, 1978; Goodwin et al. 1975; Movshon et al. 1978b; Sillito 1975, 1977) in a rather simple model that is much more analytically manageable than network models of cortical cells (Wörgötter and Koch, 1991).

The large number of inputs that converge onto one cortical cell (Freund et al. 1985a,b; Martin 1988) suggests that even the well-distinguishable ON- or OFF-subfields in fact consist of a multitude of "microsubfields," which all contribute to the response of the subfield. This is also supported by results demonstrating that direction selectivity can be elicited within small regions of one subfield (Ganz and Felder 1984; Goodwin et al. 1975). The central idea behind this study is that all spatiotemporal mechanisms included in the model act continuously in space and time. We found, somewhat unexpectedly, that such a simple model can account for the majority of important aspects of direction selectivity and velocity tuning in cortical cells. In addition the more recently reported axial response to dot stimulation (Wörgötter and Eysel 1989) is also reproduced with our model. However, some aspects of cortical cell behavior (e.g., DS_2 cells) can be explained only with additional modifications discussed below.

Spatiotemporal mechanisms—the parameter ranges of the model

Both spatial interactions between the units of a "direction detector" and purely temporal mechanisms can contribute to direction-selective behavior (Barlow and Levick 1965; Hassenstein and Reichardt 1956). In early studies it was demonstrated that spatiotemporal feed forward of activity is involved in the generation of direction selectivity and velocity tuning (Bishop et al. 1971; Goodwin and Henry 1975). Inhibitory feed forward along the nonpreferred direction has been commonly suggested as a major mechanism (Bishop et al. 1971; Eysel et al. 1987, 1988; Sillito 1975, 1977). Facilitation along the preferred direction has also been found (Emerson and Gerstein 1977b; Movshon et al. 1978b). In most of the studies, however, a clear separation between purely temporal mechanisms (e.g., delays) and purely spatial mechanisms (e.g., distance, convergence pattern, etc.) was not made. A recent study by Reid et al. (1987) showed that direction tuning can only be achieved if the receptive fields include two asymmetries: one in the spatial and the second in the temporal domain. An example of such a mechanism is given by Soodak (1986) who modeled a directional selective field by including a phase lag between the excitatory and inhibitory regions of the subfields (Hassenstein and Reichardt 1956). Our approach makes use of the basic observation of Reid et al. (1987), and like them we found that true directional selectivity is achieved in our model only after including a strong threshold nonlinearity.

TEMPORAL DOMAIN. Cortical and subcortical cells show response latencies and low-pass behavior, both of which can contribute to a delay mechanism (Soodak 1986). The la-

tency includes multiple propagation delays between the photoreceptors and the actual cell. For cortical cells the latency to flashing bar stimulation falls within a range of 45 and 80 ms (Baker 1988). This mechanism is not modeled, and the possible effect of including it in the simulation will be discussed below.

Low-pass filtering also embodies aspects of a delay mechanism because, during stimulation with a step function, the maximum response amplitude will be reached only after a delay that is determined by the time constant of the filter. The temporal response of the population of simple cells to flashing stimuli is not homogeneous. Although the cell responses are basically linear (mostly showing the null-response to counter-phasing gratings at a given phase shift) (Movshon et al. 1978a), many of them show a fast and steep phasic component at stimulus onset and settle only after a longer time to a certain tonic response level. Phasic and tonic components are expressed with different strength throughout the entire simple cell population (Duysens et al. 1982; Ikeda and Wright 1975a,b), making it even more difficult to determine the actual low-pass filter time constant. Also, the time constant is not simply the passive membrane constant but is much longer (Baker 1988; Emerson and Gerstein 1977a; Ganz and Felder 1984), implying additional mechanisms. The most reliable estimates are obtained from curves showing the response amplitude to moving sinusoidal gratings of optimal spatial frequency at different temporal frequencies (Holub and Morton-Gibson 1981; Ikeda and Wright 1975a; Movshon et al. 1978c). Cells in area 17 show low-pass behavior with a −3-dB falloff at ~2–3 Hz, corresponding to time constants of 53–80 ms. Most of the simulation results were obtained within this parameter range, although we have also included rather long time constants (maximum 160 ms) to show extreme cases.

SPATIAL DOMAIN. Experimental evidence suggests that spatial interactions exist within the receptive field (Bishop et al. 1971). For example, inactivation of small regions of cortical tissue at ~1 mm lateral distance of the cell under study can result in an altered direction specificity (Eysel et al. 1988). Near the projection equivalent of the area centralis, a distance of 1 mm represents the outer regions of the receptive field. Also, the results of Henry et al. (1978) show that there is a nonlinear contrast dependency of the response to two simultaneously flashed bars. Furthermore, an experiment using simultaneously flashed double bars was done by Heggelund (1986a,b), which clearly indicates a nonlinear spatial interaction.

None of these experiments clearly shows the shape of the interaction; for this reason we chose to use a decaying exponential because it is computationally simple even though it excludes a specific long-range connections as those described by Gilbert (for a review see Gilbert 1985). The spatial interaction constant λ (see *Eq. 3*) is varied between 0 and 2°, corresponding to many of the findings about interactions between (or within) subfields (Bishop et al. 1971; Duysens 1987; Ganz and Felder 1984; Heggelund 1986b; Jones 1970).

MAPPING THE MODEL ONTO LGN AND CORTEX. Without doubt, the model is an oversimplification of the complicated cortical network. Because it is meant to implement general mechanisms that are likely to exist within this network, its basic task is not to reproduce the structure of the cortex [for such an approach see Wörgötter and Koch, (1991)]. Nevertheless, several features of the cortical network are inherently present in our simple model. For example, it is very likely that velocity low-pass cells reflect a simpler computational level than velocity-tuned cells (see Orban 1984). Accordingly, velocity low-pass behavior can already be obtained from the cells in the intermediate level in Fig. 1, whereas only the top level cell exhibits velocity tuning. Furthermore, the cells in the intermediate level also exhibit orientation-selective behavior because they receive input from a row of LGN cells (Hubel and Wiesel 1962). Thus the model does not require unoriented cortical cells, in agreement with cat data. In addition, as long as we assume that any feedback connection strength in the cortex is small (which is likely given the high convergence), the straight feed-forward architecture of our model can approximate the realistic cortical network, which also contains feedback (Shamma 1989). In general, there exists a trade off between the transparency of a model and its realistic detail. The analytic approach taken here enables us to investigate some basic mechanisms while at the same time to implement the model so that a coarse mapping onto LGN and cortex is still possible.

Relationship between direction selectivity and velocity tuning

Visual cortical cells are classified as velocity broadband, low-pass, high-pass, or tuned (Orban 1984; Orban et al. 1981a). [Only three classes are used for direction selectivity: nondirection-selective (NDS $MDI < 50$), direction asymmetric (DA; $50 < MDI < 66$), and direction selective (DS $MDI \geq 66$)]. According to Orban and co-workers (Orban 1984; Orban et al. 1981a,b), most velocity-tuned cells are DS. Table 1 shows this and also that the other classes (velocity low-pass, high-pass, and broadband) are predominantly NDS or DA. Also, velocity high-pass cells constitute only a small minority of the cells in area 17 of the cat (Orban 1984; Orban et al. 1981a); in monkey area V1, no velocity high-pass cells are found at all (Orban et al. 1986). Therefore we excluded velocity high-pass cells from our study, although we observed that eliminating the last low-pass filtering step in the model results in a high-pass behavior (not shown).

Orban (1984) discusses velocity low-pass behavior as a passive cell property in which the smaller response to larger velocities reflects only the shorter duration of stimulus exposure with increasing velocity. Velocity low-pass cells are, in fact, generated by the model using only the low-pass mechanism. Depending on the values for τ, a simulated cell will behave like either a velocity low-pass or a broadband cell, so the division between these two classes is continuous in the model. In real cells this division is not as pronounced as the division between these two groups and the velocity-tuned cells (Movshon 1975; Orban 1984; Orban et al. 1981a). Figure 4 shows a DA velocity low-pass cell (Fig. 4*A*) and a NDS velocity broadband cell (Fig. 4*B*). In principle, any combination of NDS and DA cell behavior with velocity low-pass or broadband tuning can be achieved with

the model varying τ and the shape of the receptive field (σ_x, f_0). However, achieving true DS with low values of τ (i.e., in velocity broadband cells) requires unrealistic spatial parameter settings. It is much more likely that DS velocity broadband cells are generated by convergence of many DS velocity-tuned cells with uniformly distributed optimal velocities.

Simulated DA cells behave according to the synergy model for direction selectivity (Hubel and Wiesel 1962), reversing their preferred direction when the stimulus contrast is reversed. DS and DA cells constitute 54% of all (simple and complex) cells in area 17 (Orban 1984); according to different reports, ~15–40% of the simple cells are DA-type cells (Ganz and Felder 1984; Orban 1984; Pettigrew et al. 1968). The clear majority of the real DA cells are velocity low-pass or broadband cells (Table 1) and show reversal of the preferred direction when the stimulus contrast is reversed (Bishop et al. 1974).

Velocity-tuned cells are predominantly strongly DS (Orban 1984). DS cells make up 30–60% of the simple-cell population (Ganz and Felder 1984; Orban 1984; Pettigrew et al. 1968). They have been subdivided into DS_1 and DS_2 cells according to their response to contrast reversal of the bar stimulus (Ganz and Felder 1984). Ganz and Felder (1984) found that 31% of DS cells (in their study 24.6% of the simple cells) respond to only a light or a dark stimulus (DS_1 cell behavior). The model reproduces this with phase-shifted odd symmetrical Gabor fields and a threshold (which also improves directional selectivity).

DS_2 cells respond with the same preferred direction to light and dark bars. About 20% of the cells show this behavior (Ganz and Felder 1984), which cannot be simulated by our model. However, summing two DS_1 cells with receptive fields phase shifted by $\phi = 180°$ would result in DS_2 behavior.

Problem of spatiotemporal separability

Our model has two levels of complexity that are reflected by either excluding or including the mechanism of activity distribution. Without activity distribution it is not necessary to consider the top-level cell in Fig. 1, because the cells in the intermediate level basically produce the same DA velocity low-pass behavior as the top-level cell. The equations that generate this behavior (*Eqs. 1–4*) reflect a system that is separable in space and time. It is conceivable that the separable cells observed by Baker and Cynader (1988) belong to this category. Unfortunately, no clear account on the actual direction selectivity of the cells is given in this report, which seems to conflict with the observation of McLean and Palmer (1989). They find that predominantly nonseparable cells exhibit true direction selectivity. However, it is possible that both studies subsample the cortical cell population and that, in fact, separable receptive fields are associated with low direction tuning, whereas nonseparability is accompanied by strong direction selectivity. This is also suggested by our model. We do not get direction selectivity without introducing the activity distribution mechanism with its associated thresholds, i.e., only after implementing a nonseparable receptive field (Adelson and Bergen 1985).

Dot responses

Visual cortical cells respond more strongly to a dot moving along the long axis of the receptive field than to a dot moving across (Wörgötter and Eysel 1989). Because this response can even be stronger than the response to an optimal flashing bar, it has been suggested that temporal facilitation is involved. The temporal mechanisms in the model enable it to reproduce this behavior. Also, depending on the shapes of the Gabor functions for the receptive fields, some unusual tuning curves regarding superposition of the bar and dot responses are reproduced (Fig. 9). This shows that a dot response is a fairly straightforward result, which can probably be achieved with the majority of linear filter models that include temporal interactions.

The transition from the bar response into the orthogonally oriented dot response was not sufficiently explained in the previous report (Wörgötter and Eysel 1989). In particular, it remained unclear why some cells seem to show a preferred axis of motion for the dot <90° apart from that for the bar. Both results can be entirely explained by the model if the center of stimulus rotation is offset from the center of the receptive field. The older statement (Henry et al. 1974a), that dots and bars apparently have the same preferred axis of motion but different tuning strength, is also explained by the model if, in addition, the dots are too large.

Wörgötter and Eysel (1989) also show examples of cells with an asymmetrical response for a moving dot. In these cells the response is larger for motion in one direction along the receptive-field long axis than for motion in the opposite direction. Such a behavior was predominantly found in "end-stopped" cells and indicated the existence of inhibitory end-zones with different strength on either end of the receptive field. This behavior could be easily introduced in the model by the use of modified Gabor functions with a periodicity also along the y-axis of the receptive field.

The model predicts that the optimal velocity for the dot is significantly higher than that for the bar. This effect is presumably due to the elongation of the receptive field. It has been observed that cells with wider receptive fields have higher optimal velocities for bars. In analogy to this, the optimal velocity for a dot measured along the long axis of the receptive field is larger than the optimal velocity for a bar that is measured along the short axis. Furthermore, the tuning strength for the dot increases with increasing velocity, whereas for the bar it decreases (Fig. 12). This effect was strong in the simulated velocity-tuned cells and much weaker in velocity low-pass cells (~25% of the effect in velocity-tuned cells).

Improving the model—additional mechanisms

Including a response latency would not change the qualitative behavior of the model. Shorter time constants could be used in the low-pass filter, resulting in a sharper onset of the response.

Adaptation effects in cortical cells lead to continuous reduction of the response during prolonged stimulus presentation. In some cells the response can be completely eliminated after a while. The time constants for adaptation are

rather long (Baker 1988), so this effect is probably important only for very slow velocities.

Including discontinuities in the spatiotemporal interactions is probably the most interesting way to improve the model. It is a crude approximation in our model to assume that the distribution of activity is isotropic. It might be more realistic to assume inhibition is distributed only in the nonpreferred direction, and facilitation only in the preferred direction. Isotropic distribution of activity results in a velocity-tuned behavior along the preferred *and* the nonpreferred direction. Most cells, however, show velocity low-pass behavior in the nonpreferred direction (Orban 1984). This could be easily achieved by assuming that spatiotemporal interactions occur only along the preferred direction. However, analytical implementation of an anisotropic filter function complicates the model to an extent that extinguishes the model's basic merit, its simplicity.

Direction selectivity can be generated in cortical cells even with very small stimulus displacements (Ganz and Felder 1984; Goodwin et al. 1975). This shows that even with a subfield there is substructure. The continuous spatial-temporal interactions included in the current model partly account for such behavior. There are, however, indications that inhibitory interactions can be elicited even within an excitatory region. This suggests that inhibitory cells converge onto the cell under study with a receptive field that overlaps its excitatory zone. The amplitude of the inhibition, however, it not sufficient to eliminate the excitatory response, so the overall response of that part of the field is excitatory, but it may be strong enough to modify it. Such a behavior could only be included in a model by subdividing the receptive field. Doing so would lose the original intention of implementing an analytic form for the receptive field.

Caveats and conclusions

We show that a relatively limited analytic model, which includes only basic spatiotemporal filter mechanisms, can reproduce many of the features of cortical simple cells in the spatial and temporal domain. Some aspects of simple-cell behavior cannot be directly reproduced with the model (e.g., DS velocity broadband cells or DS_2 cells), but simple patterns of convergence of the model neurons, as discussed above, would result in these types of behavior. Also, it is obvious that several more complicated nonlinearities reported even for simple cells cannot be reproduced with this model. The basic mechanisms implemented in our model are probably supplemented by more complicated interactions in real cells. For example, the high (sub- and intracortical) convergence onto cortical cells may inherently lead to more pronounced nonlinear behavior, if for no other reason than the multiple thresholds involved. [For example, Suarez and Koch (1989) show that a quadratic behavior can be achieved with multiple linear threshold units.] Such modification of the current model would increase the parameter space and lead away from an analytic model toward a network model. The central advantage of the transparency of this model will definitely be reduced by such steps. Rather, it seems more reasonable to use this model as a *basic DS and velocity-sensitive simple-cell module* in network approaches toward more complicated (e.g., complex) cell behavior.

The authors are grateful to U. Eysel, R. Freeman, F. Perez, H. Suarez, and D. Van Essen for critical comments on the approach and the manuscript. In particular, we thank C. Koch for many fruitful discussions. F. Wörgötter was supported by Grant Wo 388-1 of the Deutsche Forschungsgemeinschaft, Federal Republic of Germany. The authors gratefully acknowledge the support from the Air Force Office of Scientific Research and of a NSF Presidential Young Investigator Award and funds from the James S. McDonnell Foundation to C. Koch.

Address for reprint requests: F. Wörgötter, Institut für Physiologie, Ruhr-Universität Bochum, D-4630 Bochum, Federal Republic of Germany.

Received 8 January 1990; accepted in final form 25 October 1990.

REFERENCES

ADELSON, E. H. AND BERGEN, J. R. Spatiotemporal energy models for the perception of motion. *J. Opt. Soc. Am.* 2: 284–299, 1985.

BAKER, C. L. Spatial and temporal determinants of directionally selective velocity preference in cat striate cortex neurons. *J. Neurophysiol.* 59: 1557–1574, 1988.

BAKER, C. L. AND CYNADER, M. S. Spatial receptive field properties of direction selective neurons in cat striate cortex. *J. Neurophysiol.* 55: 1136–1152, 1986.

BAKER, C. L. AND CYNADER, M. S. Space-time separability of direction selectivity in cat striate cortex neurons. *Vision Res.* 28: 239–246, 1988.

BARLOW, H. B. AND LEVICK, W. R. The mechanism of directionally selective units in rabbit's retina. *J. Physiol. Lond.* 178: 477–506, 1965.

BISHOP, P. O., COOMBS, J. S., AND HENRY, G. H., Interaction effects of visual contours on the discharge frequency of simple striate neurones. *J. Physiol. Lond.* 219: 659–687, 1971.

BISHOP, P. O., GOODWIN, A. W., AND HENRY, G. H. Direction selective sub-regions in striate simple cell receptive fields (Abstract). *J. Physiol. Lond.* 238: 25–27P, 1974.

DAUGMAN, J. G. Two-dimensional spectral analysis of cortical receptive field profiles. *Vision Res.* 20: 847–856, 1980.

DAUGMAN, J. G. Spatial visual channels in the Fourier plane. *Vision Res.* 24: 891–910, 1984.

DEVALOIS, K. K., DEVALOIS, R. L., AND YUND, E. W. Responses of striate cortical cells to grating and checkerboard patterns. *J. Physiol. Lond.* 291: 483–505, 1979.

DUYSENS, J. Is direction selectivity of cat area 17 cells always independent of contrast and dependent on short-distance interactions? *Exp. Brain Res.* 67: 663–666, 1987.

DUYSENS, J., MAES, H., AND ORBAN, G. A. The velocity dependence of direction selectivity of visual cortical neurones in the cat. *J. Physiol. Lond.* 387: 95–113, 1987.

DUYSENS, J., ORBAN, G. A., AND CREMIEUX, J. Velocity selectivity in the cat visual system. II. Independence from interactions between different loci. *J. Neurophysiol.* 54: 1050–1067, 1985a.

DUYSENS, J., ORBAN, G. A., CREMIEUX, J., AND MAES, H. Velocity selectivity in the cat visual system. III. Contribution of temporal factors. *J. Neurophysiol.* 54: 1068–1083, 1985b.

DUYSENS, J., ORBAN, G. A., AND VERBEKE, O. Velocity sensitivity mechanisms in cat visual cortex. *Exp. Brain Res.* 45: 285–294, 1982.

EMERSON, R. C. AND GERSTEIN, G. L. Simple striate neurons in the cat. I. Comparison of responses to moving and stationary stimuli. *J. Neurophysiol.* 40: 119–135, 1977a.

EMERSON, R. C. AND GERSTEIN, G. L. Simple striate neurons in the cat. II. Mechanisms underlying directional asymmetry and directional selectivity. *J. Neurophysiol.* 40: 136–155, 1977b.

EYSEL, U. T., MUCHE, T., AND WÖRGÖTTER, F. Lateral interactions at direction-selective striate neurones in the cat demonstrated by local cortical inactivation. *J. Physiol. Lond.* 399: 657–675, 1988.

EYSEL, U. T., WÖRGÖTTER, F., AND PAPE, H.-C. Local cortical lesions abolish lateral inhibition at direction selective cells in cat visual cortex. *Exp. Brain Res.* 68: 606–612, 1987.

FIELD, D. J. AND TOLHURST, D. J. The structure and symmetry of simple-cell receptive-field profiles in the cat's visual cortex. *Proc. R. Soc. Lond. B Biol. Sci.* 228: 379–400, 1986.

FREUND, T. F., MARTIN, K. A. C., SOMOGYI, P., AND WHITTERIDGE, D.

Innervation of cat visual areas 17 and 18 by physiologically identified X- and Y-type afferents. II. Identification of postsynaptic targets by GABA immunocytochemistry and Golgi impregnation. *J. Comp. Neurol.* 242: 275–291, 1985a.

FREUND, T. F., MARTIN, K. A. C., AND WHITTERIDGE, D. Innervation of cat visual areas 17 and 18 by physiologically identified X- and Y-type afferents. I. Arborization patterns and quantitative distribution of postsynaptic elements. *J. Comp. Neurol.* 242: 263–274, 1985b.

GABOR, D. Theory of communication. *J. IEE Lond.* 93: 429–457, 1946.

GANZ, L. AND FELDER, R. Mechanism of directional selectivity in simple neurons of the cat's visual cortex analyzed with stationary flash sequences. *J. Neurophysiol.* 51: 294–324, 1984.

GILBERT, C. D. Horizontal integration in the neocortex. *Trends Neurosci.* 8: 160–165, 1985.

GOODWIN, A. W. AND HENRY, G. H. Direction selectivity of complex cells in a comparison with simple cells. *J. Neurophysiol.* 38: 1524–1540, 1975.

GOODWIN, A. W. AND HENRY, G. H. The influence of stimulus velocity on the responses of single neurones in the striate cortex. *J. Physiol. Lond.* 277: 467–482, 1978.

GOODWIN, A. W., HENRY, G. H., AND BISHOP, P. O. Direction selectivity of simple striate cells: properties and mechanism. *J. Neurophysiol.* 38: 1500–1523, 1975.

GRAY, C. M., KÖNIG, P., ENGEL, A. K., AND SINGER, W. Oscillatory responses in cat visual cortex exhibit inter-columnar synchronization which reflects global stimulus properties. *Nature Lond.* 338: 334–337, 1989.

HAMMOND, P. Directional tuning of complex cells in area 17 of the feline visual cortex. *J. Physiol. Lond.* 285: 479–491, 1978.

HARTLINE, H. K. The response of single optic nerve fibers of the vertebrate eye to illumination of the retina. *Am. J. Physiol.* 121: 400–415, 1938.

HASSENSTEIN, B. AND REICHARDT, W. Systemtheoretische Analyse der Zeit- Reihenfolgen- und Vorzeichenauswertung bei der Bewegungsperzeption des Rüsselkäfers. *Chlorophanus. Z. Naturf.* 11b: 513–524, 1956.

HEGGELUND, P. Quantitative studies of enhancement and suppression zones in the receptive field of simple cells in cat striate cortex. *J. Physiol. Lond.* 373: 293–310, 1986a.

HEGGELUND, P. Quantitative studies of the discharge fields of single cells in cat striate cortex. *J. Physiol. Lond.* 373: 277–292, 1986b.

HENRY, G. H., BISHOP, P. O., AND DREHER, B. Orientation, axis and direction as stimulus parameters for striate cells. *Vision Res.* 14: 767–777, 1974a.

HENRY, G. H., DREHER, B., AND BISHOP, P. O. Orientation specificity of cells in cat striate cortex. *J. Neurophysiol.* 37: 1394–1409, 1974b.

HENRY, G. H., GOODWIN, A. W., AND BISHOP, P. O. Spatial summation of responses in receptive fields of single cells in cat striate cortex. *Exp. Brain Res.* 32: 245–266, 1978.

HOLUB, R. A AND MORTON-GIBSON, M. Response of visual cortical neurons of the cat to moving sinusoidal gratings: response-contrast functions and spatiotemporal interactions. *J. Neurophysiol.* 46: 1244–1259, 1981.

HUBEL, D. H. AND WIESEL, T. N. Receptive fields, binocular interaction and functional architecture in the cat's visual cortex. *J. Physiol. Lond.* 160: 106–154, 1962.

IKEDA, H. AND WRIGHT, M. H. Spatial and temporal properties of "sustained" and "transient" neurones in area 17 of the cat's visual cortex. *Exp. Brain Res.* 22: 363–383, 1975a.

IKEDA, H. AND WRIGHT, M. H. Retinotopic distribution, visual latency and orientation tuning of "sustained" and "transient" cortical neurones in area 17 of the cat. *Exp. Brain Res.* 22: 385–398, 1975b.

JONES, B. H. Responses of single neurons in cat visual cortex to a simple and a more complex stimulus. *Am. J. Physiol.* 218: 1102–1107, 1970.

JONES, J. P. AND PALMER, L. A. The two-dimensional spatial structure of simple receptive fields in cat striate cortex. *J. Neurophysiol.* 58: 1187–1211, 1987a.

JONES, J. P. AND PALMER, L. A. An evaluation of the two-dimensional Gabor filter model of simple receptive fields in cat striate cortex. *J. Neurophysiol.* 58: 1233–1258, 1987b.

KULIKOWSKI, J. J. AND BISHOP, P. O. Linear analysis of the responses of simple cells in the cat visual cortex. *Exp. Brain Res.* 44: 386–400, 1981.

KULIKOWSKI, J. J., MARČELJA, S., AND BISHOP, P. O. Theory of spatial position and spatial frequency relations in the receptive fields of simple cells in the visual cortex. *Biol. Cybern.* 43: 187–198, 1982.

MAFFEI, L. AND FIORENTINI, A. The visual cortex as a spatial frequency analyzer. *Vision Res.* 13: 1255–1267, 1973.

MARR, D. *Vision.* San Francisco, CA: Freeman, 1982.

MARR, D. AND HILDRETH, E. C. Theory of edge detection. *Proc. R. Soc. Lond. B* 207: 187–217, 1980.

MARČELJA, S. Mathematical description of the responses of simple cortical cells. *J. Opt. Soc. Am.* 70: 1297–1300, 1980.

MARTIN, K. A. C. From single cells to simple circuits in the cerebral cortex. *Q. J. Exp. Physiol.* 73: 637–702, 1988.

MCLEAN, J. AND PALMER, L. A. Contribution of linear spatiotemporal receptive field structure to velocity selectivity of simple cells in area 17 of cat. *Vision Res.* 29: 675–679, 1989.

MIKAMI, A., NEWSOME, W. T., AND WURTZ, R. H. Motion selectivity in macaque visual cortex. II. Spatiotemporal range of directional interactions in MT and V1. *J. Neurophysiol.* 55: 1328–1339, 1986.

MOVSHON, J. A. The velocity tuning of single units in cat striate cortex. *J. Physiol. Lond.* 249: 445–468, 1975.

MOVSHON, J. A., DAVIS, E. T., AND ADELSON, E. H. Directional movement selectivity in cortical complex cells. *Soc. Neurosci. Abstr.* 6: 670, 1980.

MOVSHON, J. A., THOMPSON, I. D., AND TOLHURST, D. J. Spatial summation in the receptive fields of simple cells in the cat's striate cortex. *J. Physiol. Lond.* 283: 53–77, 1978a.

MOVSHON, J. A., THOMPSON, I. D., AND TOLHURST, D. J. Receptive field organization of complex cells in the cat's striate cortex. *J. Physiol. Lond.* 283: 79–99, 1978b.

MOVSHON, J. A., THOMPSON, I. D., AND TOLHURST, D. J. Spatial and temporal contrast sensitivity of neurones in areas 17 and 18 of the cat's visual cortex. *J. Physiol. Lond.* 283: 101–120. 1978c.

ORBAN, G. A. Neuronal operations in the visual cortex. In: *Studies of Brain Function,* edited by H. B. Barlow, T. H. Bullock, E. Florey, O. J. Grüsser, and A. Peters. Berlin: Springer-Verlag, 1984, vol. 11.

ORBAN, G. A., KENNEDY, H., AND BULLIER, J. Velocity sensitivity and direction selectivity of neurons in areas V1 and V2 of the monkey: influence of eccentricity. *J. Neurophysiol.* 56: 462–480, 1986.

ORBAN, G. A., KENNEDY, H., AND MAES, H. Response to movement of neurons in areas 17 and 18 of the cat: velocity sensitivity. *J. Neurophysiol.* 45: 1059–1073, 1981a.

ORBAN, G. A., KENNEDY, H., AND MAES, H. Response to movement of neurons in areas 17 and 18 of the cat: direction selectivity. *J. Neurophysiol.* 45: 1043–1058, 1981b.

PETTIGREW, J. D., NIKARA, T., AND BISHOP, P. O. Responses to moving slits by single units in cat striate cortex. *Exp. Brain Res.* 6: 373–390, 1968.

POLLEN, D. A. AND RONNER, S. F. Visual cortical cells as localized spatial frequency filters. *IEEE Trans. SMC* 13: 907–915, 1983.

REID, R. C., SOODAK, R. E., AND SHAPLEY, R. M. Linear mechanisms of directional selectivity in simple cells of cat striate cortex. *Proc. Natl. Acad. Sci. USA* 84: 8740–8744, 1987.

SHAMMA, S. Spatial and temporal processing in auditory networks. In: *Methods in Neuronal Modeling,* edited by C. Koch and I. Segev. Cambridge, MA: *MIT Press,* 1989, p. 247–290.

SILLITO, A. M. The contribution of inhibitory mechanisms to the receptive field properties of neurones in the striate cortex of the cat. *J. Physiol. Lond.* 250: 287–304, 1975.

SILLITO, A. M. Inhibitory processes underlying the directional specificity of simple, complex and hypercomplex cells in the cat's visual cortex. *J. Physiol. Lond.* 271: 669–720, 1977.

SKOTTUN, B. C., GROSOF, D. H., AND DE VALOIS, R. L. Responses of simple and complex cells to random dot patterns: a quantitative comparison. *J. Neurophysiol.* 59: 1719–1735, 1988.

SOODAK, R. E. Two-dimensional modeling of visual receptive fields using Gaussian subunits. *Proc. Natl. Acad. Sci. USA* 83: 9259–9263, 1986.

SUAREZ, H. AND KOCH, C. Linking linear threshold units with quadratic models of motion perception. *Neural computation* 1: 318–320, 1989.

WÖRGÖTTER, F. AND EYSEL, U. T. Axis of preferred motion is a function of bar length in visual cortical receptive fields. *Exp. Brain Res.* 76: 307–314, 1989.

WÖRGÖTTER, F., AND KOCH, G. A detailed model of the primary visual pathway in the cat. Comparison of afferent excitatory and intracortical inhibitory connection schemes for orientation selectivity. *J. Neurosci.* In press.